Available online at www.sciencedirect.com

ScienceDirect

Solar Energy 119 (2015) 310–318

SOLAR ENERGY

www.elsevier.com/locate/solener

Simulation of a passive solar dryer to charqui production using temperature and pressure networks

G. Duran, M. Condorí*, F. Altobelli

Instituto de Investigaciones en Energía No Convencional, Concejo Nacional de Investigaciones Científicas y Técnicas, Universidad Nacional de Salta, Av. Bolivia 5150, A4408FVY Salta, Argentina

Received 3 December 2014; received in revised form 1 May 2015; accepted 1 July 2015
Available online 24 July 2015

Communicated by: Associate Editor I. Farkas

Abstract

This paper presents a passive solar dryer that includes a chimney and a wind turbine to improve the airflow rate. The prototype of 2 m^2 of drying chamber area was tested to obtain charqui (dried beef). In relation to the traditional charqui, the final quality was greatly improved and drying time was reduced to less than two sunny days. A simulation method of the passive solar dryer is also presented. In this, pressure and thermal coupled network are used to represent the dryer, and they are solved by electrical analogy. Simulation and experimental results were analyzed, showing a good fit to the measured data, especially with trends. In all cases, the fits between measured and simulated data have coefficients of determination r^2 higher than 0.93. The simulation method is suitable to be used in the design of passive solar dryers to find the optimum mass air flow.

Keywords: Passive solar dryer; Natural convection; Electric analogy; Wind turbine

1. Introduction

Open sun drying is still the most popular drying technique used in many rural areas of the Argentinian Northwest. Although inexpensive, it has considerable losses due to adverse environmental conditions and the exposure to animals and insect attack. In addition, the final quality of dried product is reduced due to the pollution with dust, fungi, solar radiation burns and animal remains.

Different solar dryer designs have been proposed to overcome the shortcomings of open sun drying and these efforts have required improved technology (Ayensu, 1997; Bala et al., 2003; Condorí et al., 2001a; Hossain et al., 2005). In solar dryer design, natural or forced convection of air is used for evacuating humid from drying chamber, being the forced convection the safest method to implement but also the most expensive.

As many rural areas in the world have poor access to the electric grid, in these places the solar dryers are usually of the passive type. These dryers have the minor load capacity, since the product, geometry and singularities in the dryer produce pressure drops that are not conducive to the airflow rate with natural convection. Hence, an optimized design to improve airflow and drying speed is needed in passive dryers (Afriyie et al., 2011; Ekechukwu and Norton, 1997, 1999; Fudholi et al., 2010; Pangavhane et al., 2002; Pangavhane and Sawhney, 2002).

The mechanism driving air circulation in passive systems is well known. Although there are models of varying grades of complexity, the standard method considers only the buoyancy force of the air (ASHRAE, 1989; Etheridge

* Corresponding author. Tel.: +54 387 4255424.
E-mail address: miguel.angel.condori@gmail.com (M. Condorí).

http://dx.doi.org/10.1016/j.solener.2015.07.002
0038-092X/

Nomenclature

A_b	inner plate area
A_{ch}	charqui area
A_p	cover area
C_a	thermal storage in air
C_b	thermal storage in chamber
C_{ch}	thermal storage in charqui
EP_{amb}	pressure source to fix a reference pressure
ET_{am}	temperature source for ambient temperature
ET_{sky}	temperature source for sky temperature
Gr	Gashof's number
h_a	convective coefficient in inner chamber
$h_{rch\text{-}b}$	thermal radiation resistance charqui-inner plate
$h_{rp\text{-}b}$	thermal radiation resistance cover-inner plate
$h_{rp\text{-}ch}$	thermal radiation resistance cover-charqui
$h_{rp\text{-}s}$	thermal radiation resistance upper cover-sky
h_w	wind convective coefficient
J_a	heat source by mass air flow
J_{ev}	heat source by charqui evaporation
Jm_{ch}	mass airflow source due to wind turbine
Jm_{wind}	mass airflow source due to solar chimney
J_{rb}	heat source by solar radiation on inner plate
J_{rch}	heat source by solar radiation on charqui
J_{rp}	heat source by solar radiation on cover
Pai	air pressure in ith node
P_{amb}	the reference pressure, atmospheric
Ra	Rayleigh's number
R_{DCelb}	air pressure resistance due to contraction
R_{DSI}	air pressure resistance due to chamber entry
R_{DSch}	air pressure resistance due to charqui
R_{DSelb}	air pressure resistance due to 90° coupling
R_{DSout}	air pressure resistance at the outlet of chimney
Re	Reynold's number
R_{FRch}	air pressure resistance due to friction in chamber
R_{FRchim}	air pressure resistance due to friction in chimney
T_a	airflow temperature in dryer
T_{amb}	ambient temperature
T_b	chamber inner plate temperature
T_{ch}	charqui temperature
T_p	cover temperature
T_{sky}	sky temperature
Δx	chamber thickness

and Sandberg, 1996; Ong, 2003). In this, the pressure gain is directly proportional to the air density difference between the chimney and the environment, at the same height.

$$\Delta p = gH(\rho_a - \rho_{ch}) \quad (1)$$

where g is the acceleration of gravity, ρ is the air density and H is the chimney height.

In a solar dryer, there are other passive ways of generating airflow as when wind turbine or solar chimney is used. Design tools for passive solar dryers are scarce and fewer consider the generation of airflow. In order to establish the equations to passive dryer different methods of determining airflow in ventilation systems were considered (Awbi, 1994; Krope and Goricanec, 1991; Mathews and Rousseau, 1994) and the mass flow network procedures by forced solar dryer was mainly followed (Imre, 1987). Based on those, coupled pressure and temperature networks were taken as most suitable for passive solar dryer simulation.

2. The passive solar dryer

In the north of the Argentine, the meat is still drying through its exposition to environmental conditions. This product is known with the native name of "charqui" and the required drying time is around a week. Due to dust and insect contamination, a low quality dried product is obtained. A passive solar dryer with solar chimney was built to improve the traditional solar technology used in the charqui production.

The dryer consisted of a drying chamber (2 m long, 0.8 m wide and 0.1 high) and a union elbow (0.4 m long and 0.1 high). This elbow reduced the chamber rectangular section to a circular one, where a chimney (1 m high and 0.15 m diameter) were added with a wind turbine at its top. The chimney was built with galvanized steel tube and was painted matte black. A removable door with air filter was placed at the front of the chamber. In addition, the elbow was removable to permit the access by both ends and simplified the loading and cleaning of the chamber. This had a small pipe in the door where the excess of blood can be extracted by gravity, improving the energy use and the drying time. The outside body of the chamber was constructed with galvanized sheet and the inner with stainless sheet folded, both separated by glass wool of 2.5 cm thick. The drying chamber was closed with an upper cover of transparent alveolar polycarbonate (4 mm thick). The union elbow was also built in galvanized sheet.

The wind turbine employed was locally manufactured. It was built in aluminum and has an aspiration diameter of 150 mm. It is impulse by wind drafts, and therefore, it does not require electrical supply. The mean estimated flow is about 800 m^3/h according to the manufacturer.

The dryer load capacity was 4 kg/m^2 of fresh meat placed on trays. In the chamber, a unique level of plastic mesh tray was placed at mid-height so the air could flow over and under the meat. Solar radiation reaches the meat

Fig. 1. Photo of passive solar dryer. Back of chamber with elbow union, chimney and wind turbine (left); front part of chamber with plastic tray (right).

through a transparent cover increasing its temperature and improving the drying time. Due to the low humidity in the region, the dryer works during the night helped by the wind turbine. In Fig. 1, photos of different parts of the passive solar dryer are shown.

The dryer is positioned with a slight slope of approximately 10° and it is moved several times a day facing sun and tracking the solar azimut. The reason for this slope is to improve the blood exit by gravity. This slope can be changed according to the sun altitude and improving the collection. However, it was decided to adopt a conservative attitude toward the slope in order to avoid increasing the product temperature, and to facilitate the product manipulation.

3. The networks

Next, simulation of the passive solar dryer using the method of electrical network analogy is presented. This is carried out by solving two coupled networks, the thermal and the pressure networks for air flow.

3.1. Temperature network

The method of electrical analogy was applied to represent heat transfers in the dryer (Duffie and Beckman, 2006), considering the following general equation:

$$Q_i = \frac{(T_i - T_{i+1})}{R_i} \tag{2}$$

where Q_i is the rate heat transfers (in Watt), T_i is a generic temperature node of the network, R_i is the thermal resistance between two adjacent temperature nodes and it takes different expressions according to the heat transport type.

$$R_i = \frac{P}{A_i h_i} \tag{3}$$

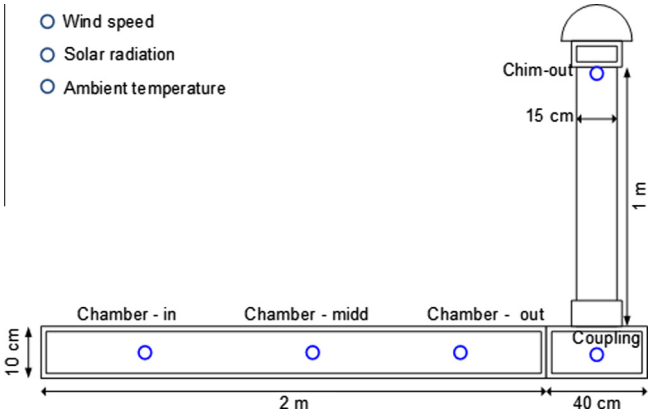

Fig. 2. Scheme of passive solar dryer with the dimensions of its parts. The air temperature nodes used in the thermal network.

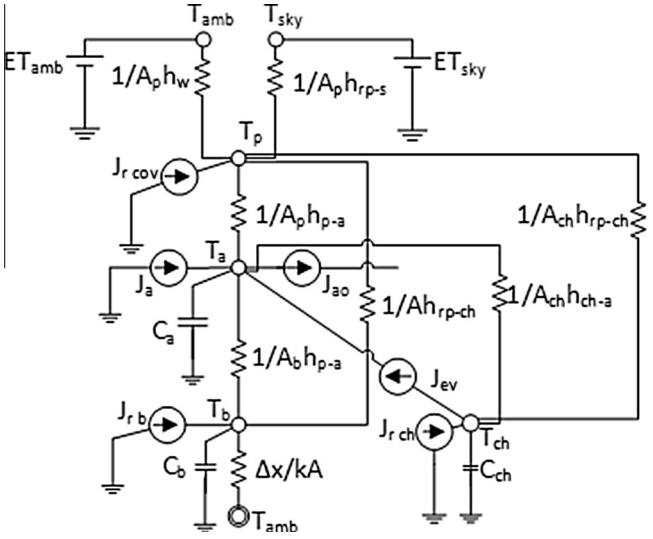

Fig. 3. Network temperature nodes for the first section of drying chamber of the passive solar dryer.

where A_i is the area for transfer and h_i is the corresponding heat transfer coefficient. $P = 1$ in case of heat transfer by radiation or convection (W/m^2 K) and when $P = \Delta x$, the wall thickness, h_i becomes the heat transfer by conduction coefficient k (W/m K).

A scheme of the passive solar dryer is shown in Fig. 2, including the representative air temperature nodes. The drying chamber was divided into three equal sections. In Fig. 3, the thermal network corresponding to the first section is shown. In this section, the inner air temperature is equal to the ambient temperature; in the other two sections, the air reaches with the temperature obtained in the previous section. Solar radiation on a horizontal surface, wind speed and ambient temperature are the measured input data, and four self-regulated temperatures are used: air T_a, charqui T_{ch}, upper cover T_p, and inner plate of the chamber T_b.

Two nodes were associated with known temperature sources using the measured input data. One of them is the ambient temperature T_{amb} and the other one the sky temperature, T_{sky}, which is considered equal to ambient temperature minus ten degrees.

The upper cover has thermal losses toward the ambient temperature due to the wind. The wind convective coefficient is calculated by the following equation (Duffie and Beckman, 2006):

$$h_w = 5.7 + 3.8\, v \tag{4}$$

where v is the wind speed in m/s and h_w has units of W/m^2 K.

To calculate the thermal radiation losses toward sky temperature from upper cover, the following coefficient was used.

$$h_{rp\text{-}s} = \sigma \varepsilon_p (T_p^2 + T_{sky}^2)(T_p + T_{sky}) \tag{5}$$

where σ is the Stefan–Boltzmann constant and ε_p is the polycarbonate emissivity.

The heat exchange between the charqui surface and the upper cover was estimated by using the radiation coefficient for parallel plates.

$$h_{rp\text{-}ch} = \frac{\sigma (T_{ch}^2 + T_p^2)(T_{ch} + T_p)}{\frac{1}{\varepsilon_{ch}} + \frac{1}{\varepsilon_p} - 1} \tag{6}$$

where ε_{ch} represents the charqui emittance.

An equation similar to Eq. (6) was used for the thermal radiation exchange between the upper cover and the inner chamber. The effective area was estimated as the difference between total inner area and charqui area. In addition, the emittance of stainless steel sheet was used as ε_b.

It was not taken into account the heat capacity of the temperature node T_p in the polycarbonate cover, since its mass was consider as insignificant.

In drying chamber, the same coefficient was considered for the convection heat exchange between the air and upper cover, the air and the inner surfaces, and the air and the charqui.

$$h_{p\text{-}a} = \frac{Nu\, k}{D_h} \tag{7}$$

where Nu is the Nusselt number, k the air thermal conductivity and D_h the hydraulic diameter of the chamber cross section.

In the drying chamber the Reynolds and Grashof numbers are $Re < 2000$ and $Ra < 10^7$, hence Nusselt numbers for both natural and forced convection were considered in Eq. (7), as Grashof and Reynolds numbers fulfilled the following condition:

$$0.1 < Gr/Re^2 < 10 \tag{8}$$

For laminar air flow, Tan and Charters correlation was used for forced air flow between parallel plates with one side insulated and the other side subject to a constant heat flux (Duffie and Beckman, 2006).

$$Nu_{forc} = 5.4 + \frac{0.00190(RePrD_h/L)^{1.71}}{1 + 0.00563(RePrD_h/L)^{1.17}} \tag{9}$$

where L is the drying chamber length, and a Prandtl number of 0.71 was considered.

For natural convection and laminar flow with Rayleigh number ($Ra < 10^9$), the Churchill and Chu correlation was used (Incropera et al., 2006)

$$Nu_{nat} = 0.68 + 0.51 Ra^{1/4} \tag{10}$$

The following correlation was used to combine both contributions (Incropera et al., 2006):

$$Nu_{comb} = (Nu_{forc}^3 + Nu_{nat}^3)^{1/3} \tag{11}$$

Similar expression to Eqs. (7)–(11) is used with the convection transfer in the inner chamber and charqui surfaces. Moreover, the air temperature nodes have input and output of mass air flow. These are considered as an energy source by the following equation:

$$J_a = \dot{m}_a C_p (T_{ai+1} - T_{ai}) \tag{12}$$

The input of solar radiation was considered as a tension and current source. The source J_i represents the total solar radiation that actually reaches on the chamber inner plate and it is expressed as follows:

$$J_{rb} = (\tau\alpha)_b A_b I_i \tag{13}$$

where A_i is the effective inner area to solar radiation, i.e. minus the charqui area, I_i is the total solar radiation on horizontal surface, the product $\tau\alpha = 0.8$ was used, where τ is the transmittance of the covers and α the absorptance of the stainless steel plate.

A similar expression was used to take into account the incident solar radiation on the charqui surface:

$$J_{rch} = (\tau\alpha)_{ch} A_{ch} I_i \tag{14}$$

The resistance by thermal conduction in the drying chamber from inner plate to ambient air, considers $\Delta x = 25$ mm thickness for the insulating material and $k = 0.04$ W/mK for the conductivity coefficient.

$$R_i = \frac{\Delta x}{A_i k_i} \tag{15}$$

For heat exchange by thermal radiation between the inner plates of the chamber and the charqui surface, the following transfer coefficient was calculated:

$$h_{rb\text{-}ch} = \frac{\sigma(T_{ch}^2 + T_b^2)(T_{ch} + T_b)}{\frac{1}{\varepsilon_{ch}} + \frac{1}{\varepsilon_b} - 1} \tag{16}$$

where ε_b is the sheet steel emittance.

The charqui temperature node has the same heat transfer coefficients mentioned above and solar radiation gain similar to Eq. (10), except that the solar collection area is A_{ch}, the charqui area.The energy required to convert water into steam with speed $\dot{m}_w$ is, $l_{eV}\dot{m}_w$ where l_{ev} (kJ kg^{-1}) is the water evaporation latent heat (Altobelli et al., 2014). Once the evaporation occurs, and steam is incorporated, the air gains energy. In the model, the energy gain is considered for a convective coefficient, and for the energy flow Jm.

The following equation is proposed to express the flow Jm:

$$Jm = C_d l_{eV} \dot{m}_w \tag{17}$$

where coefficient C_d is an adjustment variable of the model, $l_{ev} = 2.5 \times 10^6$ J/kg is the latent heat of evaporation and m_w the evaporation rate. The latter is obtained from Eq. (18). Eq. (18) is the drying velocity definition in dry weight base, which is expressed in kg/s of evaporated water (Mujumdar, 1997):

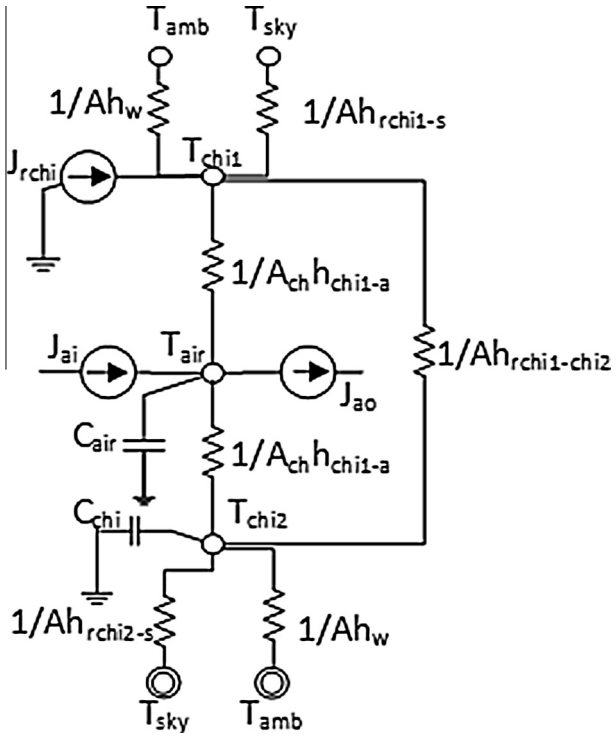

Fig. 4. Network temperature nodes for the chimney of the passive solar dryer.

$$\dot{m}_w = -P_d \frac{dX(t)}{dt} \tag{18}$$

where P_d is the dried weight of charqui and $X(t)$ the drying curve in dried basis.

In Fig. 4, the network corresponding to chimney is shown. Because they are similar, the network of the elbow union is not analyzed. On the chimney, since measured solar radiation was on the horizontal plane the solar radiation is affected by Rb, the ratio of beam radiation on chimney to that on the chamber. The absorptance of the black-painted galvanized sheet was taken as $\alpha = 0.7$.

Into the chimney, $Re < 10^4$ and $Ra < 10^9$ and the airflow is forced and turbulent. Most of the time, the condition of Eq. (8) was fulfilled so that natural and forced Nusselt numbers were added using Eq. (9) to obtain the convection coefficient of Eq. (19).

$$h_{chi\text{-}a} = \frac{Nu\ k}{D} \tag{19}$$

where D is the chimney diameter.

The Dittus–Boelter equation for developed forced flow and cooling was used (Cengel, 1998),

$$Nu_{fch} = 0.023 Re^{0.8} Pr^{0.3} \tag{20}$$

For natural and turbulent flow with $Ra > 10^9$, the following equation was used (Afriyie et al., 2011; Incropera et al., 2006):

$$Nu = \left(0.825 + 0.321 Ra_L^{1/6}\right)^2 \tag{21}$$

where L is the chimney length.

3.2. Pressure network

In the pressure network model, the air movement arises from the difference of pressure between two adjacent nodes and the obstacles to airflow were considered as resistors. Moreover, the pressure at a node can be increased by airflow sources as chimney effect or a wind turbine.

In general, the pressure difference between any two nodes of the network is determined according to the following equation:

$$\Delta p = \sum \Delta p^+ - \sum \Delta p^- \tag{22}$$

where Δp is the pressure difference between nodes, $\Sigma \Delta p^+$ is the total pressure gain due to airflow sources, $\Sigma \Delta p^-$ corresponds to the total pressure drop produced by the airflow resistance. Although the pressure distribution may not be uniform, mean values per node were considered.

The mass flow rate $\dot{m}$ is expressed in terms of the airflow velocity v by its definition:

$$\dot{m} = \rho v A_T \tag{23}$$

where A_T is the cross section of duct and ρ the air density.

The pressure drops are of two kinds: friction against duct walls or particular features of the structure. The

Darcy–Weisbach equation estimates the pressure loss due to friction as follows:

$$\Delta p = R_{FR}\dot{m} \tag{24}$$

$$R_{FR} = \frac{f}{2\rho A_T^2}\left(\frac{L}{D}\right)\dot{m} \tag{25}$$

where L is the duct length, D the hydraulic diameter, and f the loss factor.

Pressure drops caused by duct singularities (such as opening, widening and curves) were estimated multiplying the dynamic pressure (expressed according to Eq. (23)) by the corresponding loss coefficient (ASHRAE, 1989):

$$\Delta p_i = R_{DS}\dot{m} \tag{26}$$

$$R_{DS} = \frac{C_i}{2\rho A_T^2}\dot{m} \tag{27}$$

where Δp_i is the pressure drop and C_i is the corresponding loss coefficient. The latter is a dimensionless number obtained experimentally which depended on the geometry of the singularity and the Reynolds' number. Information on usual geometries is available in ASHRAE (1989).

Eqs. (24) and (26) are expressed similarly to Ohm's Law. Thus, the mass air flow rate is analogous to the electric current, pressure difference equals the voltage difference and the Eqs. (25) and (27) represents resistances, that are functions of the mass air flow.

The airflow sources need to overcome pressure drops to create air movement. There are different ways to induce airflow. In this work, only two of them were considered: chimney effect and wind turbine.

The following simplified equation was used in the case of a simple chimney (Condorí et al., 2001b), where a unidirectional flow is considered:

$$Jm_{ch} = C_D A_T[\rho_h g\, H(\rho_a - \rho_h)]^{0.5} \tag{28}$$

where H is the chimney height, A_T its cross area, C_D the discharge coefficient (0.65 was used), ρ_h the air density at the chimney outlet and ρ_a the ambient air density.

In the case of wind turbine, a linear relation between airflow Q and wind speed v was considered. Manufacturers usually provide curves for this relation. The origin ordinate of this line was not taken into account since it wrongly indicates the existence of airflow even in windless situations. This ordinate value is actually caused by the stack effect.

Thus, the following expression for the mass air flow rate is considered for a wind turbine:

$$Jm_{wind} = C_D\rho_h(pv) \tag{29}$$

where C_D is the discharge coefficient (0.5 was considered), ρ_h is the air density at the extractor outflow vent and p is the slope of the linear relation between airflow and wind speed obtained in the working range.

The pressure network corresponding to the passive dryer is shown in Fig. 5. Each node corresponds to the pressure of the air with resistances in between; these are

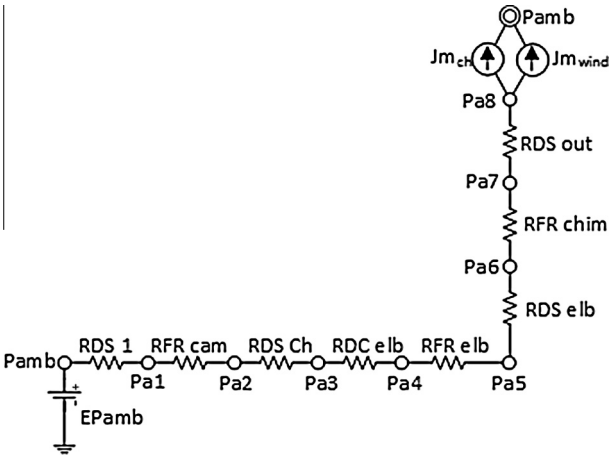

Fig. 5. Scheme of pressure network for the passive solar dryer.

pressure drops occurring along the dryer. On the output, the circuit has the two airflow sources connected in parallel, which produce the air movement.

The atmospheric pressure on Salta city, P_{amb}, was taken as the reference because of this the corresponding node is connected with a pressure source EP_{amb}.

The simulation required simultaneous resolution of pressure and temperature networks, since the airflow is governed by air density differences. The software SIMUSOL, (Alias et al., 2012), was used as computer tool to solve both networks. The mathematical calculus engine is Sceptre, simulation software for electric circuits, and DIA was the drawing software used for diagramming the circuits.

4. Experimental tests

The tests were carried out with the passive dryer, on a sunny winter day around solar midday in Salta City (24°48′ Lat S, 65°25′ Long W), in the north of Argentina. The following variables were measured in the trials: ambient temperature, air flow temperature in the drying chamber, air flow temperature in the chimney, global solar radiation on the cover plane, airflow rate at the chimney exit, and the wind speed.

A Campbell Sci CR 32x datalogger of 12 differentials channels was used for data recording. The temperature measures were performed with calibrated K type thermocouples, that have a relative error of 3%. To protect the temperature sensors against possible disturbances caused by the heat exchange between different internal surfaces, a cylinder of reflective aluminum was placed around each of them. The radiation measurements were carried out using a Kipp&Zonnen CM3 pyranometer, with an expected accuracy for daily sums of ±10%. The airflow measurements were performed with a hot-wire anemometer TSI VelociCalc 8345, with a 0.01 m/s accuracy, a response time of 2000 ms, and an accuracy of ±1.5%. For wind speed measurement it was employed a cup anemometer

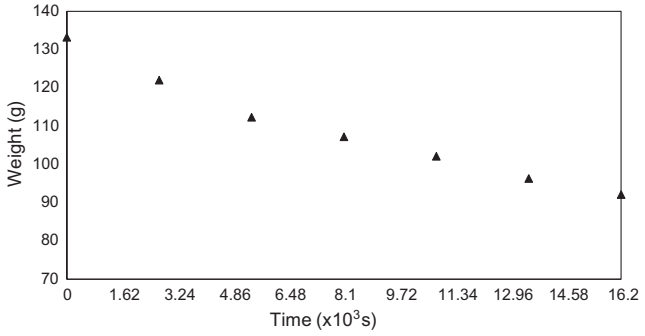

Fig. 6. Weight variation of beef charqui for 4.5 h of the first day of working. The initial weight of the sample was 0.133 kg.

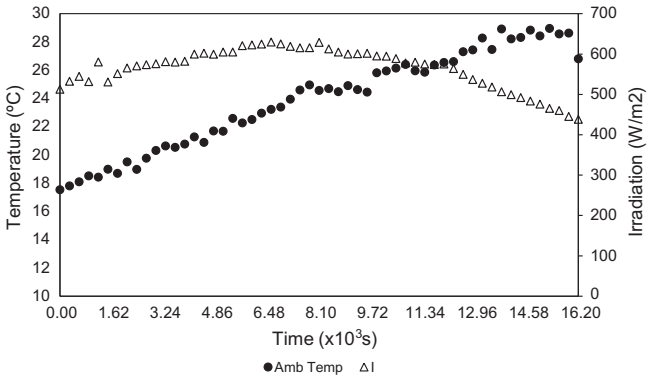

Fig. 7. Data of incident solar radiation on horizontal surface and ambient temperature for the time test.

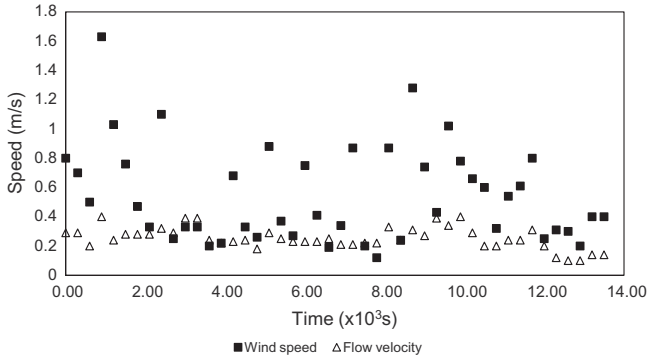

Fig. 8. Measured wind speed and airflow velocity in the chimney.

Hart Scientific 14D, with an accuracy of ±1.5%. The mass measurement were taken with a Ohaus Scout Pro Balance SPx202 with an error of 0.01 g.

In Fig. 6, weight variation with time of a sample of 0.133 kg of beef is shown. Only 4.5 h are represented, which correspond to the first day of drying. The sample lost approximately 0.043 kg of water during this time, representing more than the 50% of its initial moisture content.

Under normal operating conditions, two sunshine days were required for the production of charqui, with a yield of 1 kg of dried per 3 kg of fresh. The charge density was

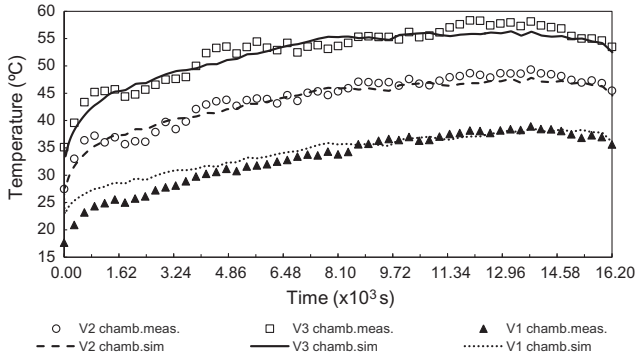

Fig. 9. Comparison between the simulated and measured airflow temperatures at inlet, middle and outlet section of drying chamber.

4 kg/m^2, considering a slice thickness of 1 cm. The sample lost about 0.013 kg of water in the first hour, being this drying rate almost constant during the whole experiment.

The evaporation velocity can be obtained from Fig. 6, using Eq. (18), as minus the derivative of instantaneous weight change, since the dried weight is a constant value.

The experiment length was of 4.5 h (16,200 s). The drying process was stopped when aspect and texture of the meat sample were considered appropriated. The meat temperature was not measured, however, in any time the temperature inside the dryer was above 60 °C. The simulated temperature values for the charqui were around 55–75 °C, following the trend that was observed in the air measured results.

Fig. 7 shows the measured values of ambient temperature and solar radiation on the cover dryer plane. In Fig. 8, the wind speed and airflow velocity at the exit of the chimney are also shown. The mean wind velocity for that day was around 3.4 m/s.

5. Results and discussion

The simulation was performed considering transient conditions. It was considered a temporal model based on an implicit integration routine. The simulation time was 16,200 s, that matches with the experiment length. The minimum time step used was 1×10^{-4} times the simulation time, according to the integration routine.

In Fig. 9, simulated and measured values for air temperatures at the inlet, middle and outlet sections of drying chamber are shown. The simulated curves are softer than the measured ones, but the same trend and a good agreement are observed between both results. In Fig. 10, measured and simulated values at chimney exit are shown together with the corresponding to the last chamber section. The air temperature in chimney diminishes respect to chamber due to the wind action. The fitting obtained between values is as similar to that obtained in the previous cases.

In Fig. 11, the evolution in time of the error defined as $E = (\mathrm{Vs} - \mathrm{Vm})/\mathrm{Vm}$ for data of Figs. 9 and 10 are shown.

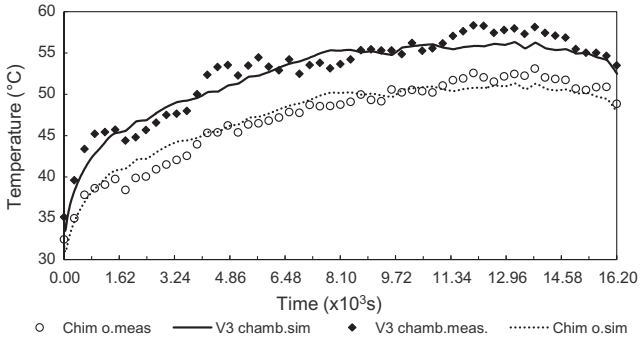

Fig. 10. Simulated and measured airflow temperatures at the chimney exit and the last (3rd) section of drying chamber.

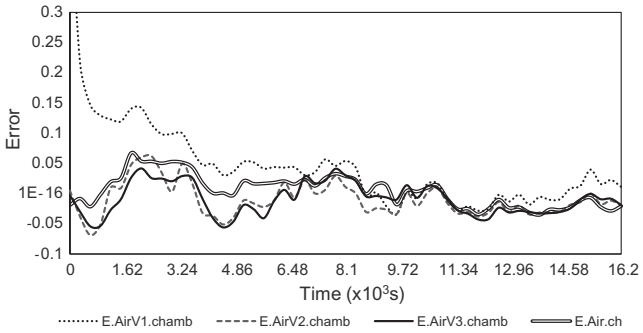

Fig. 11. Error between simulated and measured values for the airflow temperatures at drying chamber and chimney.

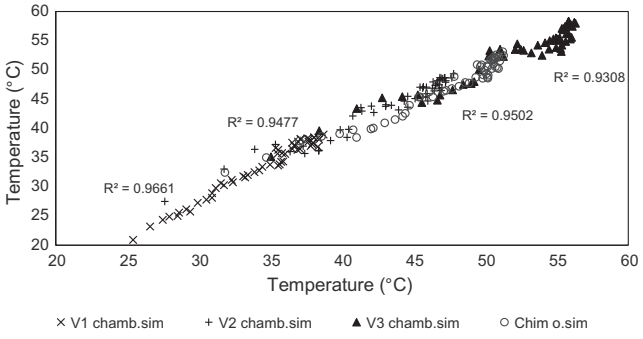

Fig. 12. Linear regressions in the three sections of drying chamber and chimney. The respective determination coefficient r^2 is shown.

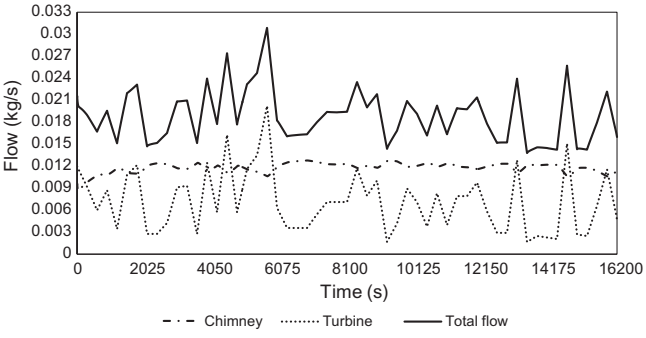

Fig. 13. Total air flow and air flow due to chimney effect and wind turbine.

The greater dispersion points appear at the beginning of the simulation, possibly due to transitory effects. After that, the settings are very good. In Fig. 12 the linear regression fits are shown. In this, coefficient $r^2 = 0.96$, 0.94 and 0.93, for the input section, middle and exit of the drying chamber, are obtained. Similar results are obtained in the chimney exit data with $r^2 = 0.95$.

Fig. 13 shows the contributions to the total flow due to the use of the wind turbine extractor, and the chimney effect was added. It can be observed that the chimney effect is the main source of airflow in the dryer, and thus, the wind turbine represents an improvement on the circulating air of around 50% of the total. However, the inclusion of the wind turbine allows extending the use of the dryer to night hours, when the ambient relative humidity is inferior to 50%.

6. Conclusion

The tested solar dryer allowed a considerable improvement in the final quality of the dried product and in the drying time, reducing it to an average of two days of sun. The air circulation was also improved by placing a wind turbine directly to the solar chimney outlet. The air flow rate provided by both devices was complemented, allowing the drying process to continue at night, when the ambient relative humidity was low, by using the wind extractor.

The meat is degreased before drying to prevent microbian grow and to perform a first blood extraction. The device has been designed to avoid temperatures that were too high for the meat, in any case the temperature was above 75 °C.

A simple tool to design of passive solar dryer was presented. Passive devices such as chimney and wind turbine were incorporated as airflow source. The simulation required the simultaneous solution of both thermal and pressure networks of the dryer. The electrical analogy method was used to solve both networks through the specific computer software SIMUSOL.

The simulated and experimental results have a very good fit. High determination coefficient of linear regression, r^2 bigger than 0.93, were obtained in all cases. An acceptable agreement in trends was observed, but the simulation was only validated for the first drying day. Since it is the most important time for the design purposes, the simulation can be used as tool design for air flow determination and optimization for passive solar dryer. Even more, while this simulation tool was applied only to passive solar dryer, it could also be used in other systems of natural or forced air circulation.

The observed reduction in drying times was due to a combination of improvements in: the constructive aspects of the dryer, the thermal isolation, the airflow that passes up and down the trays, and also to the fact that the meat on the trays worked as absorber since the stainless steel bottom is more reflective than absorptive. The wind turbine inclusion allowed to extend the functioning time of

the dryer to night hours when the ambient relative humidity conditions were appropriate, and allowed to improve the air circulation speed during day hours in relation to a passive dryer.

References

Afriyie, J.K., Rajakaruna, H., Nazha, M.A.A., Forson, F.K., 2011. Simulation and optimization of the ventilation in a chimney-dependent solar crop dryer. Sol. Energy 85, 1560–1573.

Alias, D., Saravia, L.R., Saravia, D., 2012. Simusol: simulating thermal systems using sceptre and DIA. J. Free Software Free Knowl. 1, 30–34.

Altobelli, F., Condorí, M., Durán, G., Martínez, C., 2014. Solar dryer efficiency considering the total drying potential. Application of this potential as a resource indicator in north-western Argentina. Sol. Energy 105, 742–759.

ASHRAE Handbook: Fundamentals, 1989. Infiltration and Ventilation. American Society of Heating, Refrigerating and Air Conditioning Engineers, Atlanta.

Awbi, H.B., 1994. Design considerations for naturally ventilated buildings. Renew. Energy 5, 1081–1090.

Ayensu, A., 1997. Dehydration of food crops using a solar dryer with convective heat flow. Sol. Energy 59, 121–126.

Bala, B.K., Mondol, M.R.A., Biswas, B.K., Das Chowdry, B.L., Sanjai, S., 2003. Solar drying of pineapple using solar tunnel drier. Renew. Energy 28, 183–190.

Cengel, Y., 1998. Heat Transfer: A Practical Approach, International Edition. McGraw-Hill Companies Inc.

Condorí, M., Echazú, R., Saravia, L., 2001a. Solar drying of sweet pepper and garlic using the tunnel greenhouse drier. Renew. Energy 22, 447–460.

Condorí, M., Mealla, L., Saravia, L., 2001b. Estudio y modelización de un nuevo diseño de chimenea solar. Av. Energ. Renov. Medio Ambiente 5, 19–24.

Duffie, J., Beckman, W., 2006. Solar Engineering of Thermal Processes, third ed. John Wiley and Sons, Madison.

Ekechukwu, O.V., Norton, B., 1997. Design and measured performance of a solar chimney for natural-circulation solar-energy dryers. Renew. Energy 10, 81–90.

Ekechukwu, O.V., Norton, B., 1999. Review of solar energy drying systems II: an overview of solar drying technology. Energy Convers. Manage. 40 (6), 16–55.

Etheridge, D., Sandberg, M., 1996. Building Ventilation: Theory and Measurement. John Wiley and Sons, Chichester, UK.

Fudholi, A., Sopian, K., Ruslan, M.H., Alghoul, M.A., Sulaiman, M.Y., 2010. Review of solar dryers for agricultural and marine products. Renew. Sustain. Energy Rev. 14, 1–30.

Hossain, M.A., Woods, J.L., Bala, B.K., 2005. Optimization of solar tunnel drier for drying of chilli without color loss. Renew. Energy 30, 729–742.

Imre, L.L., 1987. Simulation of solar dryers. In: Mujundar, A.S. (Ed.), Handbook of Industrial Drying. Marcel Dekker, New York, pp. 399–412.

Incropera, F.P., DeWitt, D.P., Bergamn, T.L., Lavine, A.S., 2006. Fundamentals of Heat and Mass Transfer, sixth ed. John Wiley and Sons, Madison.

Krope, J., Goricanec, D., 1991. Analysis of pipe networks including pumps. Energy Buildings 17, 141–145.

Mathews, E.H., Rousseau, P.G., 1994. A new integrated design tool for naturally ventilated buildings Part 1: Ventilation model. Build. Environ. 29, 461–471.

Mujumdar, A.S., 1997. Drying fundamentals. In: Baker, C.G.J. (Ed.), Industrial Drying of Foods. Blackie Academic & Professional, London, pp. 7–30.

Ong, K.S., 2003. A mathematical model of a solar chimney. Renewable Energy 28, 1047–1060.

Pangavhane, D.R., Sawhney, R.L., Sarsavadia, P.N., 2002. Design, development and performance testing of a new natural convection solar dryer. Energy 27, 579–590.

Pangavhane, D.R., Sawhney, R.L., 2002. Review of research and development work on solar dryers for grape drying. Energy Convers. Manage. 43, 45–61.